

Article

Epigenetic-Hydrothermal Fluorite Veins in a Phosphorite Deposit from Balaton Highland (Pannonian Basin, Hungary): Signatures of a Regional Fluid Flow System in an Alpine Triassic Platform

Zsuzsa Molnár ^{1,*}, Gabriella B. Kiss ^{1,*} , Ferenc Molnár ² , Tamás Váczi ^{1,3}, György Czuppon ⁴, István Dunkl ⁵, Federica Zaccarini ⁶ and István Dódony ¹

- ¹ Department of Mineralogy, Eötvös Loránd University, Pázmány P. Street 1/C, H-1117 Budapest, Hungary; vaczi.tamas@wigner.mta.hu (T.V.); dodony@t-online.hu (I.D.)
- ² Geological Survey of Finland, Vuorimiehentie 5, P.O. Box 96, FI-02151 Espoo, Finland; ferenc.molnar@gtk.fi
- ³ Wigner Research Centre for Physics, Eötvös Loránd Research Network, Konkoly-Thege Miklós Street 29-33, H-1124 Budapest, Hungary
- ⁴ Research Centre for Astronomy and Earth Sciences, Institute for Geological and Geochemical Research, Eötvös Loránd Research Network, Budaörsi Street 45, H-1112 Budapest, Hungary; czuppon@geochem.hu
- ⁵ Geoscience Center, Department of Sedimentology and Environmental Geology, University of Göttingen, Goldschmidtstrasse 3, D-37077 Göttingen, Germany; istvan.dunkl@geo.uni-goettingen.de
- ⁶ Department of Applied Geosciences and Geophysics, University of Leoben, Peter Tunner Street 5, A-8700 Leoben, Austria; federica.zaccarini@unileoben.ac.at
- * Correspondence: molnarzsuzsa89@gmail.com (Z.M.); gabriella.b.kiss@ttk.elte.hu (G.B.K.)



Citation: Molnár, Z.; Kiss, G.B.; Molnár, F.; Váczi, T.; Czuppon, G.; Dunkl, I.; Zaccarini, F.; Dódony, I. Epigenetic-Hydrothermal Fluorite Veins in a Phosphorite Deposit from Balaton Highland (Pannonian Basin, Hungary): Signatures of a Regional Fluid Flow System in an Alpine Triassic Platform. *Minerals* **2021**, *11*, 640. <https://doi.org/10.3390/min11060640>

Academic Editor: Joel E. Gagnon

Received: 19 April 2021

Accepted: 12 June 2021

Published: 16 June 2021

Publisher's Note: MDPI stays neutral with regard to jurisdictional claims in published maps and institutional affiliations.



Copyright: © 2021 by the authors. Licensee MDPI, Basel, Switzerland. This article is an open access article distributed under the terms and conditions of the Creative Commons Attribution (CC BY) license (<https://creativecommons.org/licenses/by/4.0/>).

Abstract: The middle Anisian extensional tectonics of the Neotethyan realm developed a small, isolated carbonate platform in the middle part of the Balaton Highland (western Hungary), resulted in the deposition of uranium-bearing seamount phosphorite on the top of the drowned platform and produced some epigenetic fluorite veins in the Middle Triassic sequence. The stable C-O isotope data of carbonates are shifted from the typical Triassic carbonate ranges, confirming the epigenetic-hydrothermal origin of veining. Primary fluid inclusions in fluorite indicate that these veins were formed from low temperature (85–169 °C) and high salinity NaCl + CaCl₂ + H₂O type (apparent total salinity: 15.91–22.46 NaCl wt%) hydrothermal fluids, similar to parent fluids of the Alpine-type Pb-Zn deposits. These findings indicate that the Triassic regional fluid circulation systems in the Alpine platform carbonates also affected the area of the Balaton Highland. This is also in agreement with the previously established palinspatic tectonic reconstructions indicating that the Triassic carbonate and basement units in the Balaton Highland area were a part of the Southern Alpine. Similar fluorite veining in phosphorite deposits is also known in the Southern Alpine areas (e.g., Monte San Giorgi, Italy). Raman spectroscopic analyses detected H₂ gas in the vapor phase of the fluid inclusions and a defect-rich fluorite structure in violet to black colored growth zones. This unique phenomenon is assumed to be the result of interaction between the uranium-rich phosphorite and the parent fluids of the epigenetic fluorite veins.

Keywords: fluid inclusions; H₂ gas; Raman spectroscopy; C-O isotopes in carbonate; structurally disordered zones in fluorite crystals; Alpine type Pb-Zn indication

1. Introduction

The regularly revised raw material policy of the European Union calls attention to the importance of certain metals and minerals (e.g., critical raw materials) for the sustainable development of European industry. Several mineral and ore occurrences that have not been previously studied in detail have significant potential for some critical elements throughout the Circum-Pannonian Basin. Re-evaluation of historically known mineral occurrences may lead to recognition of their previously ignored raw material content as well as to

re-consideration of the mineral potential in the region. Development of new ore deposit models by re-investigation of those occurrences by application of modern concepts and research methods may reveal previously hidden exploration possibilities.

The present study focuses on a previously known uranium-bearing phosphorite occurrence at Pécsely village [1,2], which is located in the Balaton Highland area, in western Hungary. This mineral occurrence is located in the Northern Transdanubium Unit, which is an allochthonous unit originated from the Southern Alps [3–5]. The phosphorite-bearing sedimentary horizons are cut by epigenetic fluorite veins. Fluorite and fluorite-base metal vein systems with economic significance in the past also occur in other parts of the Transdanubian terrain [6]. Therefore, the occurrence of the fluorite veins at Pécsely may have significance in a regional metallogenetic context. This locality also offers a unique opportunity to investigate the mineralogical and geochemical consequences of the interaction between the phosphorite and the superimposing hydrothermal processes responsible for the formation of the fluorite veins.

Results of research presented in this paper and comparison of results with similar occurrences of fluorite-bearing veins in the region provide a new background for the evaluation of the metallogenetic context of the peculiar mineralization at Pécsely and highlight the potential role of the overprinting regional scale Alpine fluid flow systems on older mineral deposits in formation of unusual metal associations and enrichments. This paper also presents and discusses some unusual features observed at this locality, such as the presence of structurally disordered zones in fluorite crystals and the occurrence of hydrogen gas in fluid inclusions of fluorite.

2. Geological Background

2.1. Regional Geology

The study area is located in the southern part of the ALCAPA (Alpine, Carpathian, Pannonian) Megaunit [4,7] along the northern side of the Periadriatic Balaton Lineament System (PABL) in western Hungary (Figure 1a). The ALCAPA Megaunit is composed of metamorphosed Proterozoic to Mesozoic blocks of the Eastern Alps and of Paleozoic low-grade metamorphic and Southern Alpine-type Mesozoic carbonaceous sequences of the Transdanubian Mountain Range (TDMR), the Bükk Mountains, as well as the crystalline blocks of the Inner Western Carpathians [5,7,8]. The current location of the ALCAPA Megaunit within the Alp-Carpathian realm is the result of its northeastward directed lateral escapement from the Eastern Alpine collision zone [4,5,7–9]. The total 350–400 km present day offset can be attributed to the Paleogene to Mid-Late Miocene extension, lateral extrusion, and counter-clockwise rotation of the ALCAPA Megaunit [9–11]. Therefore, the Paleozoic, Mesozoic, and Paleogene units along the PABL can be regarded as allochthonous blocks in a tectonic mega-mélange, between the ALCAPA and Zagorje-Mid-Transdanubian Zone [12,13].

The uranium-bearing phosphorite occurrence at Pécsely is located in the middle part of the Balaton Highland, on the southeastern flank of the NE–SW trending synform of TDMR. In the Middle Triassic sequence of this area the Pelsonian hemipelagic basal strata of the Felsőörs Limestone are replaced here by coeval platform carbonates of the Tagyon Formation [14] (Figure 1b). This lateral facies change is explained by synsedimentary extensional tectonism that has formed half-graben type hemipelagic basins and isolated carbonate platforms [15]. As the result of a relative sea-level rise, the Pelsonian Tagyon Platform was drowned and transformed to a submarine mount (the Tagyon High); the first overlying layers above it belong to the upper Illyrian Camunum Subzone [16]. This event was followed by deposition of the upper Anisian–Ladinian sequence with phosphorite horizons and radiolarite layers on the top of the submarine mount. Phosphorites are known only at the northeastern margin of the Tagyon High, at Öreg Hill, near the village of Vászoly [17]. In contrast, radiolarites and radiolarian-rich carbonates occur more widely: in addition to the area of the Tagyon High, they are also known from the eastern part of the Felsőörs Basin located in the proximity of the high at Aszófő. The occurrence of an upper

Ladinian ammonoid assemblage in a neptunian dyke cutting through the Middle Triassic platform carbonates in the northeastern part of the Balaton Highland [16] indicates the prolongation of the extensional tectonic regime at least until the end of the Middle Triassic.

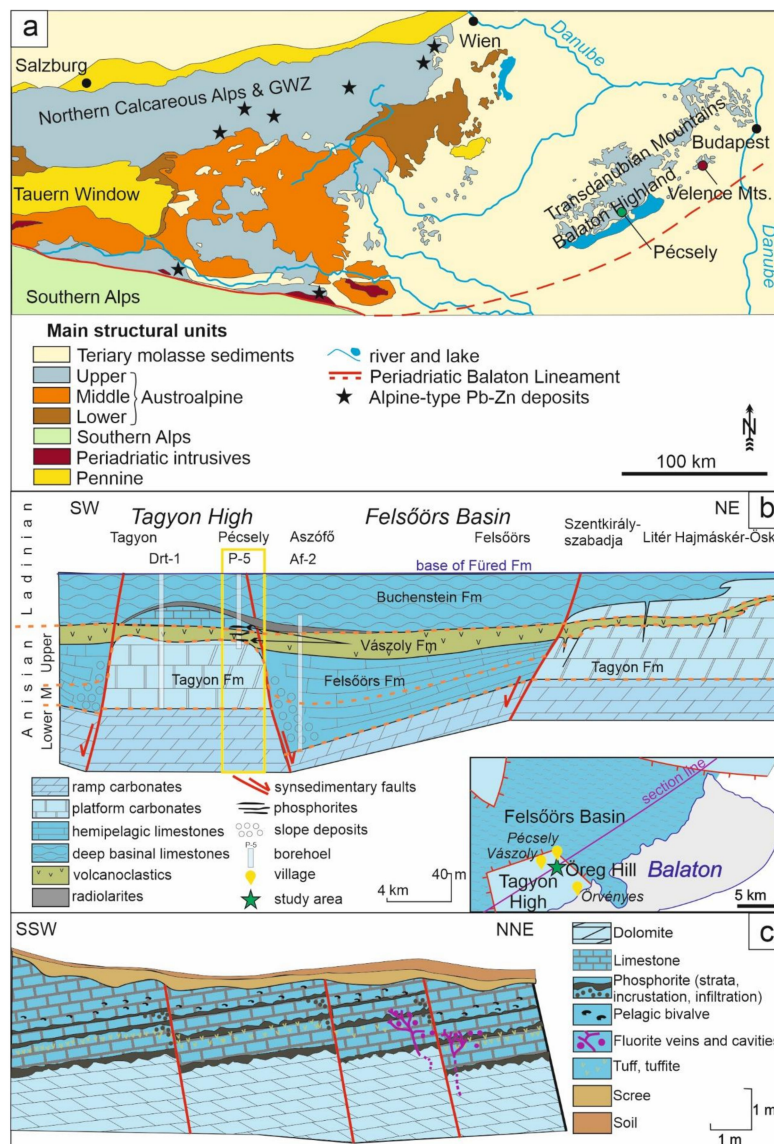


Figure 1. Location and geological structure of the study area. (a) Major structural units of the Eastern Alps—Pannonian Basin region (modified after [18]) with the positions of major Pb-Zn deposits; (b) facies arrangement of Middle Triassic Formations along the strike of the Balaton Highland [16]. The formations found in the area of Pécsely are marked with a yellow rectangle; (c) schematic geological section of the Pécsely-11 exploration trench (modified after [1]).

2.2. Geology of the Pécsely Locality

The phosphorite deposit is located at Öreg Hill, between the villages of Pécsely, Vászoly, and Örvényes (Figure 1b); GPS coordinates of the sampling site in WGS'84 (DM): N 46°55.764' E 17°47.147'). This deposit was studied in detail during the 1950s [1] due to the observed radioactive anomaly caused by the uranium content of the sedimentary phosphorite occurrence.

The phosphorite layers, together with the cross-cutting fluorite veins, are located in Triassic limestone and dolostone (Figure 1c). The host rock of the phosphorite is the Ladinian pelagic Vászoly Limestone Formation [17]. This formation is unconformably

overlying the Anisian platform carbonate Tagyon Limestone Formation deposited in a local basin and intercalated with felsic tuff in the upper Anisian [14,16].

The brownish-grey U-bearing phosphorite layers in the sedimentary sequence of the Öreg Hill appear in three horizons [2] in a less than 1 km² area. The lowermost and thickest (max. 1.2 m) horizon occurs at the drowning surface of the Tagyon Formation and the overlying tuffaceous carbonate beds of the Vászoly Formation. The middle section with varying thickness (5–20 cm) deposited after the formation of organic-rich limestone of the lower member of the Vászoly Formation. The uppermost thinnest phosphorite horizon (max 5 cm) forms a dark, greenish-grey crust on the bedding surface of the Vászoly Formation. As described by [1], fluorite-calcite veins appear along normal faults and cut across the phosphorite-rich carbonate sequence (Figure 1c).

The detailed mineralogical and geochemical characteristics of the phosphorite layers are presented in [2]. The dominant mineral assemblage in the phosphoritic layers consists of carbonate-bearing fluorapatite (CFA) and calcite, but hematite, pyrite, and zircon are also present rarely. The CFA contains 137–612 ppm U and 113–261 ppm total REE + Y. The U enrichment is related to the CFA; individual uranium-minerals were not identified. The carbon and oxygen isotopic compositions of the host limestone ($\delta^{18}\text{O}_{\text{PDB}}$ = from -2.18‰ to -1.54‰ ; $\delta^{13}\text{C}_{\text{PDB}}$ = from 1.86‰ to 1.99‰) overlap with the stable isotope field of the typical Middle Triassic marine carbonates [19], while the stable isotope values of carbonates from veins are generally characterized by different values ($\delta^{18}\text{O}_{\text{PDB}}$ = from -8.12‰ to -6.42‰ ; $\delta^{13}\text{C}_{\text{PDB}}$ = from -5.50‰ to 1.55‰) suggesting epigenetic-hydrothermal origin [2].

Earlier studies [1] suggested an epigenetic origin for the fluorite veins; however, they have left several open questions regarding the formation processes of these veins, the interaction between the phosphorite layers, and the superimposition of hydrothermal processes as well as the regional correlation with similar veins in the Transdanubian Unit.

3. Materials and Methods

In order to achieve the objectives set up during the research work, host rock, phosphorite, and fluorite vein samples were collected from the area of Öreg Hill at Pécsely (Figure 1b). Petrography of samples was carried out on standard polished thin sections using Nikon Alphaphot and Zeiss Axioplan polarizing microscopes. Qualitative SEM-EDS analyses of minerals were completed by an AMRAY 1830I scanning electron microscope. The observations were performed with 20 kV accelerating voltage and 1 nA beam current. Cathodoluminescence (CL) imaging of fluorite was performed with the same equipment using a Gatan MiniCL detector, with 10 kV accelerating voltage and 3 nA beam current. Quantitative electron microprobe analyses of the fluorite grains were completed by means of a JEOL Superprobe JXA 8200-type electron microprobe. Wavelength dispersive mode was used, with 15 kV accelerating voltage and 10 nA beam current. The detection limits for each element are shown in the related tables.

Fluid inclusion petrography and microthermometry were carried out on 100–120 μm thick, double-polished sections of hydrothermal fluorite and calcite, using a Linkam FT-IR 600 type heating–freezing stage mounted on an Olympus BX-51 type polarizing microscope providing up to 1000 times optical magnification. The calibration of the stage was done by analyses of CO₂ and pure water synthetic fluid inclusions. The precision of the microthermometric measurements was $\pm 0.1\text{ °C}$ below 0 °C , and $\pm 1\text{ °C}$ at higher temperatures. Interpretation of the microthermometric data was carried out by a macro program in MS Excel, developed in a Visual Basic environment by G. B. Kiss, using the calculation methods of salinities and isochors in [20–23].

Raman microanalyses of fluorite structure and fluid inclusions in fluorite were completed using a Horiba Jobin Yvon LabRAM HR 800 UV edge filter based confocal dispersive Raman spectrometer coupled with an Olympus BXFM type microscope. During the measurements, the 532 nm emission of a frequency-doubled Nd:YAG laser, a 600 grooves/mm grating, 50 μm confocal aperture, and 50x long working distance objective were used.

The trace element content of fluorite samples was determined by ICP-MS. Twenty-eight elements were analyzed using external calibration and U and Th by isotope dilution [24]. Single crystals of 0.5–2 mm size were gently crushed and 0.1–0.2 mm (ca. 100–200 µg), inclusion free fragments with different colors were carefully selected and dissolved in hot, ultrapure HCl. Thus, the sensitivity and spatial resolution of this technique was between the classical wet chemical analysis performed on pulverized and homogenized samples of several hundreds of mg in mass and the laser ablation technique that represents a smaller volume, but with considerably higher uncertainty. Additionally, laser ablation is typically not viable on fluorite because of the low absorption of UV light and the frequent fragmentation and small explosions during ablation. The REE distribution patterns of fluorite were compared with CI carbonaceous chondrite (CI) and Post Archean Australian Shale (PAAS) [25,26].

Carbon and oxygen isotope analyses of carbonate minerals associated with fluorite were carried out by in situ sampling of carbonates using an electric microdrill with a bit diameter of 0.6 mm. The resulting 150–200 µg samples were dissolved by carbonate-orthophosphoric acid reaction at 72 °C [27], and the aliquots were analyzed using an automated GASEBENCH II sample preparation device attached to a Thermo Finnigan Delta Plus XP mass spectrometer. The isotope compositions are expressed as $\delta^{13}\text{C}$ and $\delta^{18}\text{O}$ in ‰ relative to V-PDB (Vienna Pee Dee Belemnite), according to the equation: $\delta = (R_{\text{sample}}/R_{\text{standard}} - 1) \times 1000$, where R is the $^{13}\text{C}/^{12}\text{C}$ or $^{18}\text{O}/^{16}\text{O}$ ratio in the sample or in the international standard. The precision was better than 0.15‰ for C and O isotope data, based on replicate measurements of international standards (NBS-19; NBS-18) and in-house reference materials.

4. Results

4.1. Field Description, Mineralogy, and Petrography of the Fluorite Veins and Their Host Rock

During the field work, fluorite–dolomite–calcite veins were sampled in an abandoned pit as well as in the waste dump of that pit in the area of Öreg Hill at Pécsely (Figure 1b). The location of veins is controlled by NW–SE oriented normal faults dipping by 70° to the NE in white pinkish and white yellowish limestone, dolomitized limestone, and dolomite. The veins can be followed in a several meters long, ~10 cm wide zones along the faults. The host rocks are brecciated along the faults (Figure 2c). The thickness of the fault breccia is ~5 cm. The clasts in the monomict breccia are typically angular, rarely rounded, elongated in shape, 2 mm to 3 cm in size, which indicates movement within a short distance. The ratio of fragment to cement is 4 to 1. The crystals of fluorite, dolomite, and calcite are located around the clasts of the breccia as well as in satellite veins (Figure 2a,b). Fluorite and dolomite in the matrix of the breccia also appear in nests and cavities, in which the amount of dolomite is higher (Figure 2a,b). The fluorite grains are characterized by 0.1–2 mm size and dark purple color, and the zonation of the crystals can often be observed macroscopically. The saddle dolomite in these breccia veins is often translucent and colorless or white, but in the nests, it is always not transparent, with white or pale rose color. Textural features indicate that deposition of dolomite and calcite outlasted the crystallization of fluorite in the breccia matrix and also in the connected veinlets.

Observations in the polarizing microscope confirmed that the light pinkish color of the host rock can be related to the presence of dissemination of small flakes (2–5 µm) of hematite crystals (Figure 2a). The individual hematite flakes are rectangular and hexagonal in shape with cherry red color. Dolomite prisms are commonly corroded by hematite flakes (Figure 2b,d,e) and show undulose extinction. Microscopic observations on fluorite and dolomite showed that the outlines of these crystals are often corroded, and the grains are mostly crushed or fragmented. Individual fluorite crystals show from dark purple to colorless growth zones with all shades of purple. The SEM-CL images of fluorite also show a very fine and complicated zonation (Figure 2i,j).

The macroscopically visible dark bands consist of several thin (10–100 µm) dark purple zones (Figure 2d,e). Under crossed polarizers (+N), in contrast to the normal isotropic

behavior, these crystals do not show full extinction, and zoning in dark grey color is still visible (Figure 2e).

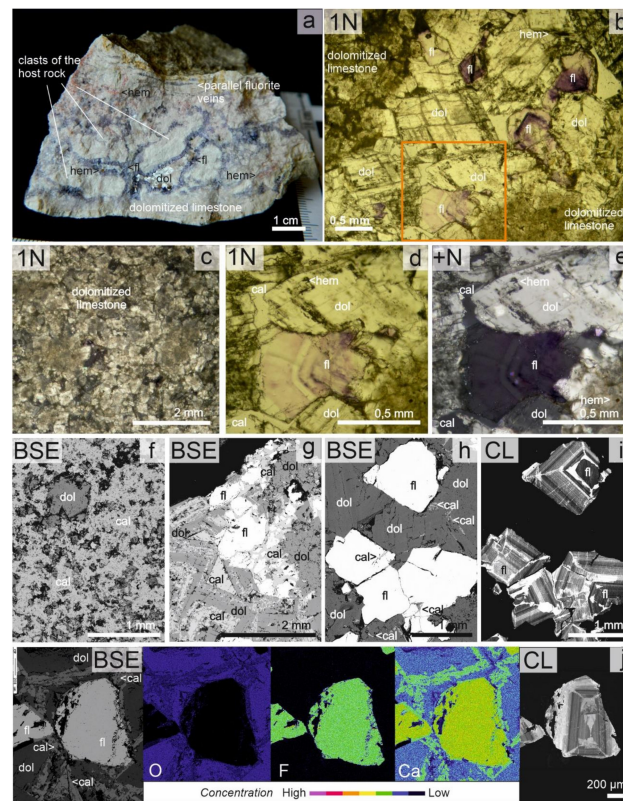


Figure 2. Mineralogy and petrography of the fluorite veins and their host rock. (a) Macroscopic picture of the contact of the fluorite–calcite–dolomite veins and host rock; (b) Microscopic picture of the fluorite–calcite–dolomite veins. The veins contain fluorite, dolomite, calcite, and hematite grains. The purple zonation of the fluorite grains is also visible. (c) Microscopic picture of the dolomitized limestone host rock; (d) microscopic image of the area indicated by an orange square in the picture b; (e) magnified microscopic image of the area indicated by an orange square in picture b. The isotropic fluorite crystals show optical anomaly (e.g., lack of full extinction) under crossed polarizers (+N) of the microscope; therefore, the zonation is visible; (f) BSE image of the host rock; (g) BSE image of fluorite and its environment. The complex dolomitization history of the vein is also visible. The fluorite grains are often fragmented, and calcite fills in the space between them; (h) BSE image of the vein-filling minerals; (i) SEM-cathodoluminescence (CL) picture of the fluorite grains and fragments; (j) BSE, element mapping and SEM-CL images of the same area. Abbreviations used: cal, calcite; dol, dolomite; fl, fluorite; hem, hematite.

Observations in the SEM revealed that the host rock limestone of phosphorite horizons and fluorite veins (Vászoly Limestone Fm.) is partly or entirely dolomitized. In the partly dolomitized rock bodies, various fabric-selective dolomite types were observed. In the beds, scattered, irregular aggregates of very finely crystalline dolomite and/or 15 to 200 μm sized euhedral, subhedral, and anhedral dolomite crystals or crystal clusters occur in the micritic fabric elements, testifying to micrite-selective dolomitization (Figure 2c). Coarsely crystalline mosaic of calcite and/or coarsely crystalline dolomite occurs in the central part of vugs (Figure 2f). In the entirely dolomitized intervals, fabric-destructive dolomite prevails, although ghosts of some calcite grains are locally recognizable. This dolomite is typically fine-to-medium crystalline, exhibiting planar-subhedral and non-planar-anhedral texture with coarsely crystalline dolomite cement in vugs. Saddle dolomite occurs locally as the last cement phase in these vugs. The carbonate minerals in the matrix of the breccia have also suffered complicated dolomitization/dedolomitization process (Figure 2g), where the saddle dolomite is dedolomitized. Furthermore, the presence of fine-grained calcite

was also observed among the fluorite grains as well as in healed microfractures of fluorite (Figure 2g,h).

Results of petrography suggest that the sequence of precipitation of the minerals was as follows: fluorite and dolomite were crystallized together at the early stages of veining, but the formation of dolomite lasted longer, and then the residual space and cracks were filled up by calcite, which also resulted in dedolomitization of the saddle dolomite. The vein filling minerals precipitated from the same fluid, which contributed to the complex dolomitization–dedolomitization history of the partly dolomitized host rock limestone.

4.2. Mineral Chemistry

The fluorite is characterized by 15–20 ppm REE + Y concentrations. All six PAAS normalized fluorite analyses show similar REE patterns (Figure 3) that are strongly depleted in light and heavy REE compared with the middle REE. They characterized low La and Ce values. All analyzed grains contained several purple zones; therefore, no correlation could be established between the color of the zones and the concentrations of analyzed elements.

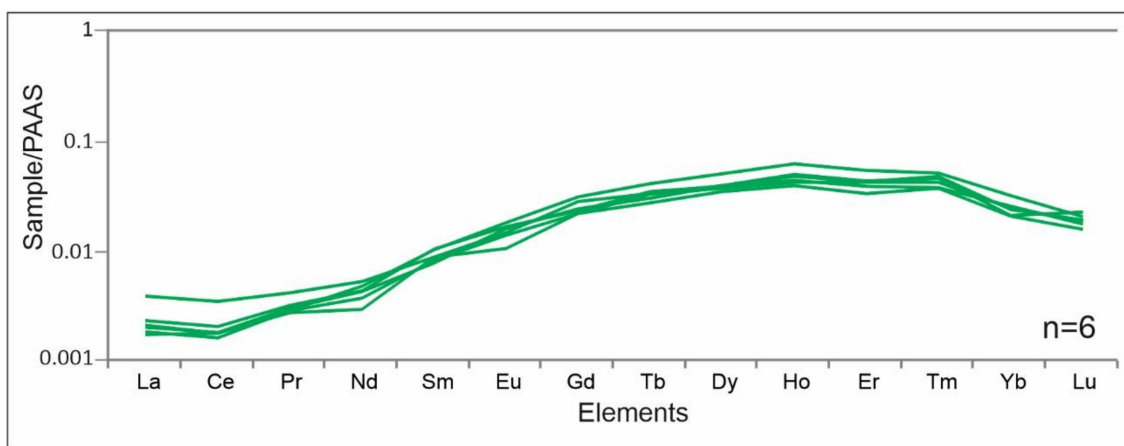


Figure 3. Post Archean Australian Shale normalized REE distribution patterns of fluorite samples from Pécseley.

4.3. Carbon and Oxygen Isotopes in Vein-Filling Carbonates

The $\delta^{18}\text{O}_{\text{PDB}}$ values range from -7.79‰ to -6.76‰ , while the $\delta^{13}\text{C}_{\text{PDB}}$ values range from -7.16‰ to 2.12‰ in the hydrothermal saddle dolomite associated with fluorite in the veins (Table 1). By comparing the obtained results with the stable isotopic composition of sedimentary carbonates precipitated in equilibrium with DIC (dissolved inorganic carbon) in Triassic seawater [19], most of the values plot outside of the marine carbonate field ($\delta^{18}\text{O}_{\text{PDB}}$ values range from -2.18‰ to -1.54‰ ; $\delta^{13}\text{C}_{\text{PDB}}$ values range from 1.86‰ to 1.99‰).

Table 1. Stable isotope data of vein filling saddle dolomite from Pécseley.

Number	$\delta^{13}\text{C}_{\text{PDB}}$ (‰)	$\delta^{18}\text{O}_{\text{PDB}}$ (‰)	Number	$\delta^{13}\text{C}_{\text{PDB}}$ (‰)	$\delta^{18}\text{O}_{\text{PDB}}$ (‰)
1	1.92	-7.46	13	-4.12	-7.36
2	1.62	-7.63	14	-3.78	-7.41
3	1.66	-7.66	15	-4.07	-7.39
4	1.57	-7.69	16	-3.05	-7.45
5	1.57	-7.58	17	-7.11	-6.93
6	-6.91	-7.12	18	-6.79	-6.78
7	-7.16	-7.15	19	-7.15	-6.92
8	-1.63	-7.54	20	-5.78	-7.36
9	-3.08	-7.50	21	1.85	-7.17
10	-5.60	-7.51	22	1.91	-6.76
11	-4.71	-7.79	23	2.12	-7.58
12	-4.24	-7.44	24	2.09	-7.53

4.4. Fluid Inclusion Petrography and Microthermometry

According to the petrographic observations, four fluid inclusion assemblages can be distinguished in fluorite: one of them consists of primary and three other assemblages consist of secondary fluid inclusions (Table 2, Figure 4a–d).

Table 2. Results of the fluid inclusion microthermometry.

	Primary	S1	Secondary S2	S3
Number of measurements	55	218	29	-
Size	5–30 μm rectangular	5–15 μm	5–30 μm	5–10 μm
Shape	(negative crystal shape)	angular	irregular	roundish
Phases	85% L + 15% V	95% L + 5% V	95% L + 5% V	100% L
T_h	85–169 $^{\circ}\text{C}$	42–121 $^{\circ}\text{C}$	45–65 $^{\circ}\text{C}$	-
T_{eut}	-57.7 to -44.0 $^{\circ}\text{C}$	-58.0 to -46.0 $^{\circ}\text{C}$	-	-
$T_{meltHydrohalyte}$	-26.5 to -21.5 $^{\circ}\text{C}$	-25.0 to -21.2 $^{\circ}\text{C}$	-	-
$T_{meltIce}$	-21.0 to -12.0 $^{\circ}\text{C}$	-20.8 to -13.7 $^{\circ}\text{C}$	-	-
Apparent total salinity	15.91–22.46 NaCl wt%	17.35–22.93 wt%	-	-
Calculated salinity	0.64–9.98 CaCl ₂ wt% + 9.59–20.64 NaCl wt%	0–8.47 CaCl ₂ wt% + 12.4–20.01 NaCl wt%	-	-

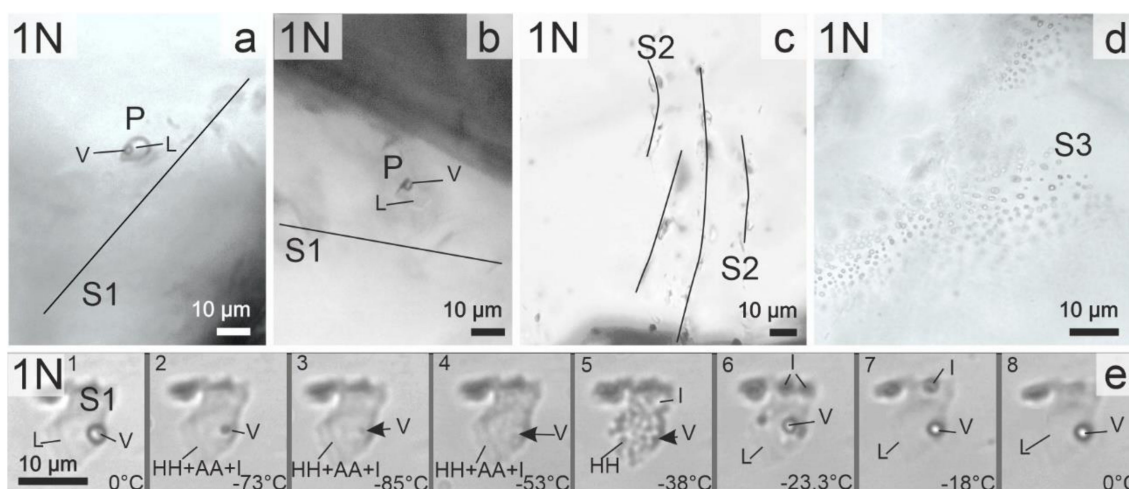


Figure 4. Fluid inclusions in fluorite. (a) Two-phased P inclusion near an S1 inclusion plane; (b) two-phased P inclusion close to a grain boundary near an S1 inclusion plane; (c) S2 two-phased inclusion generation; (d) one-phased S3 inclusion generation; (e) the behavior of an S1 inclusion during freezing. Abbreviations used: P, primary inclusion; S, secondary inclusion; L, liquid phase; V, vapor phase; HH, hydrohalite ($\text{NaCl}\cdot 2\text{H}_2\text{O}$); AA, antarctite ($\text{CaCl}_2\cdot 6\text{H}_2\text{O}$); I, ice.

The 5–30 μm large rectangular (negative crystal) shaped, aqueous, two-phase, liquid and vapor (L + V) primary inclusions (P) occur in isolation or in clusters of 2–3 small inclusions apart from the healed microcracks, along the growth zones of fluorite (Figure 4a,b). The ratio of the vapor to liquid phase is constantly around 0.15 at room temperature, indicating that these inclusions were entrapped from a homogenous parent fluid (Figure 4a,b).

The homogenization temperatures ($T_h(\text{L-V})\text{L}$) of primary fluid inclusions of the vein filling fluorite crystals are between 85 $^{\circ}\text{C}$ and 169 $^{\circ}\text{C}$ (average = 112 $^{\circ}\text{C}$, standard deviation = 20.7 $^{\circ}\text{C}$, number of analyses = 55) (Figure 5a). The average eutectic melting temperature

(T_{eut}) of the primary inclusions is $-49.8\text{ }^{\circ}\text{C}$, corresponding to NaCl–CaCl₂–H₂O type model composition (Figure 5c–e). Melting of hydrohalite (NaCl·2H₂O) occurred between $-26.5\text{ }^{\circ}\text{C}$ and $-21.5\text{ }^{\circ}\text{C}$ and the melting point of ice from -21 to $-12\text{ }^{\circ}\text{C}$, corresponding to 0.64–9.98 CaCl₂ + 9.59–20.64 NaCl wt% ($n = 8$) salinity (Figure 5e). The apparent total salinities, calculated from the ice melting temperatures using NaCl–H₂O model composition and expressed in NaCl equivalent weight%, are from 15.91 to 22.46 (Figure 5c).

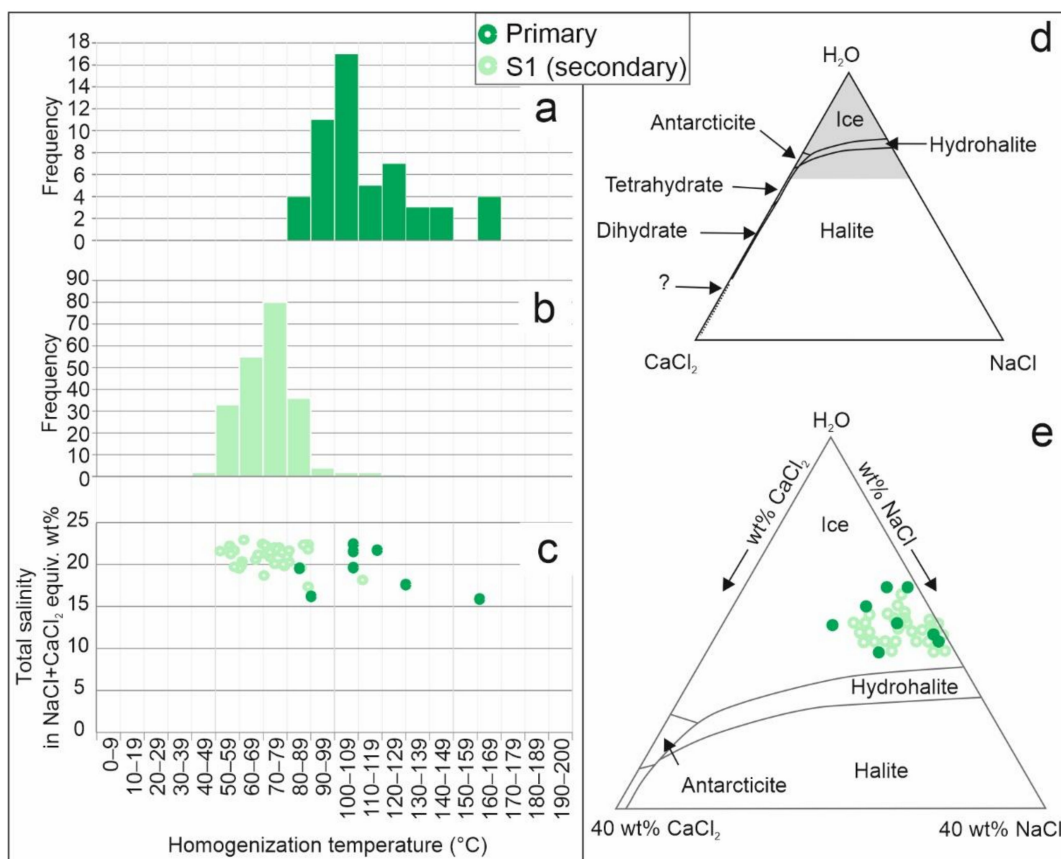


Figure 5. Results of the microthermometry study of primary (P) and S1 (secondary) fluid inclusions. (a) Frequency distribution diagram of the homogenization temperature of P inclusions; (b) frequency distribution diagram of the homogenization temperature of S1 inclusions; (c) homogenization temperature vs. total salinity diagram of P and S1 inclusions; (d) vapor-saturated liquidus phase relations in the H₂O–NaCl–CaCl₂ system [28,29]; (e) salinity compositions of aqueous inclusions trapped in fluorite from Pécsely.

The fracture/cleavage plane hosted S1 inclusions of fluorite also have an angular shape with about 5–15 μm sizes (Figure 4a,b), and the ratio of the vapor to liquid phase is around 0.05. These observations indicate entrapment from a homogenous parent fluid. Their homogenization temperature ($T_h(L-V)L$) is between 42–121 $^{\circ}\text{C}$ (average = 71 $^{\circ}\text{C}$, standard deviation = 11 $^{\circ}\text{C}$, number of measurements = 218) (Figure 5b). The average eutectic melting temperature (T_{eut}) of S1 inclusions was $-51.4\text{ }^{\circ}\text{C}$, so their composition can also be modelled in the NaCl–CaCl₂–H₂O system (Figure 4e, Figure 5c–e). The melting temperature of hydrohalite is from $-25\text{ }^{\circ}\text{C}$ to $-21.2\text{ }^{\circ}\text{C}$, and the melting temperature of ice is from $-20.8\text{ }^{\circ}\text{C}$ to $-13.7\text{ }^{\circ}\text{C}$. These data indicate that the CaCl₂ content of these inclusions is between 0–8.47 wt%, whereas the NaCl content is between 12.4–20.01 wt% (Figure 5e). The apparent total salinity calculated from melting temperature of ice and expressed in NaCl equivalent weight% using the NaCl–H₂O model system is 17.35–22.93 (Figure 5c).

The two-phase (L + V) S2 inclusions occur in fractures that have different orientations compared to the healed fractures with the S1 type of inclusions. Occurrence of S2

type inclusions is typical in fan-like inclusion planes. Inclusions in S2 fractures have irregular shapes with 5–30 μm sizes (Figure 4c). The vapor to liquid ratio is always less than 0.05; this suggests that these inclusions also entrapped a homogeneous parent fluid. The homogenization temperature of the S2 inclusion assemblage is from 45 to 65 $^{\circ}\text{C}$ (average = 55 $^{\circ}\text{C}$, standard deviation = 5.24 $^{\circ}\text{C}$) ($n = 29$). Due to the observed metastability during the microthermometry studies (e.g., disappearance of the vapor phase during freezing and melting of ice/hydrohalite in the absence of vapor phase), composition and salinities for these inclusions cannot be determined.

The S3 inclusions are filled up by a liquid phase at room temperature and their sizes are about 5–10 μm (Figure 4d) with roundish shapes. This generation of inclusions appears along large, intersecting fracture planes. No microthermometry measurements were performed on these inclusions.

4.5. Raman Spectroscopy of Fluid Inclusions and Fluorite

The fluid inclusion microthermometry study was completed by Raman spectroscopy. This method helped to check the calculated salinity values of the P and S1 inclusions (in cases where only a low amount of microthermometry data was available due to metastability) as well as aimed to determine the gas content of the vapor phase.

Based on [30,31], the O-H stretching region (2800–3800 cm^{-1}) in Raman spectra of aqueous solutions is sensitive to changes in the salt concentration. This permits determination of the salinity in the aqueous phase of fluid inclusions (at room temperature) by calculating skewing parameters from Raman microprobe spectra. In this study, the OH Raman signal is fitted using two Gaussian sub-bands, the concentration equilibrium constant was determined, then the calibration equation of Cl^{-} molarity was determined [31]. The calculated total salinity of the P inclusions was 13.9 and 19.0 NaCl equivalent wt%, and the S1 inclusions were 13.0 and 17.2 NaCl equivalent wt%. These results are in good agreement with the microthermometry data.

According to the Raman spectra of the V phase of P and S1 inclusions, they contain H_2 gas. The characteristic bands of H_2 gas are at 355, 588, 816, and 1037 cm^{-1} (Figure 6), which are related to the rotational transitions of the gas molecule.

Using Raman spectroscopy, we also aimed to investigate the relationships between fine color zoning, as well as the anomalous optical behavior and the structural state of the fluorite crystals. Colorless transparent fluorite is characterized by a single, sharp band at 318 cm^{-1} . In the dark violet zones, which also show anomalous optical behavior, broad bands appear between 80–480 cm^{-1} , and the baseline of the spectra is also elevated. This phenomenon may be explained by the changes in the structure of fluorite: the darker zones of fluorite are partly or extensively disordered, whereas the colorless and clear zones have an ordered structure (Figure 7). This phenomenon systematically occurs within the fluorite crystals. The same phenomenon was previously described for purple fluorite used as historic pigments [32]. The cause of the disorder was not identified during the recent investigation. Note, however, that the width of individual colored zones is in cases very small, approaching or possibly below the lateral optical resolution ($<1 \mu\text{m}$) of the Raman microscope. Spectra showing mixed crystalline and disordered fluorite signatures may therefore arise from the presence of damaged and ordered structures in the excitation volume. The FWHM (Full Width at Half Maximum) of fluorite bands was also examined. There is no observable band broadening near the disordered zones; hence, there is a sharp boundary between the ordered and the disordered structures.

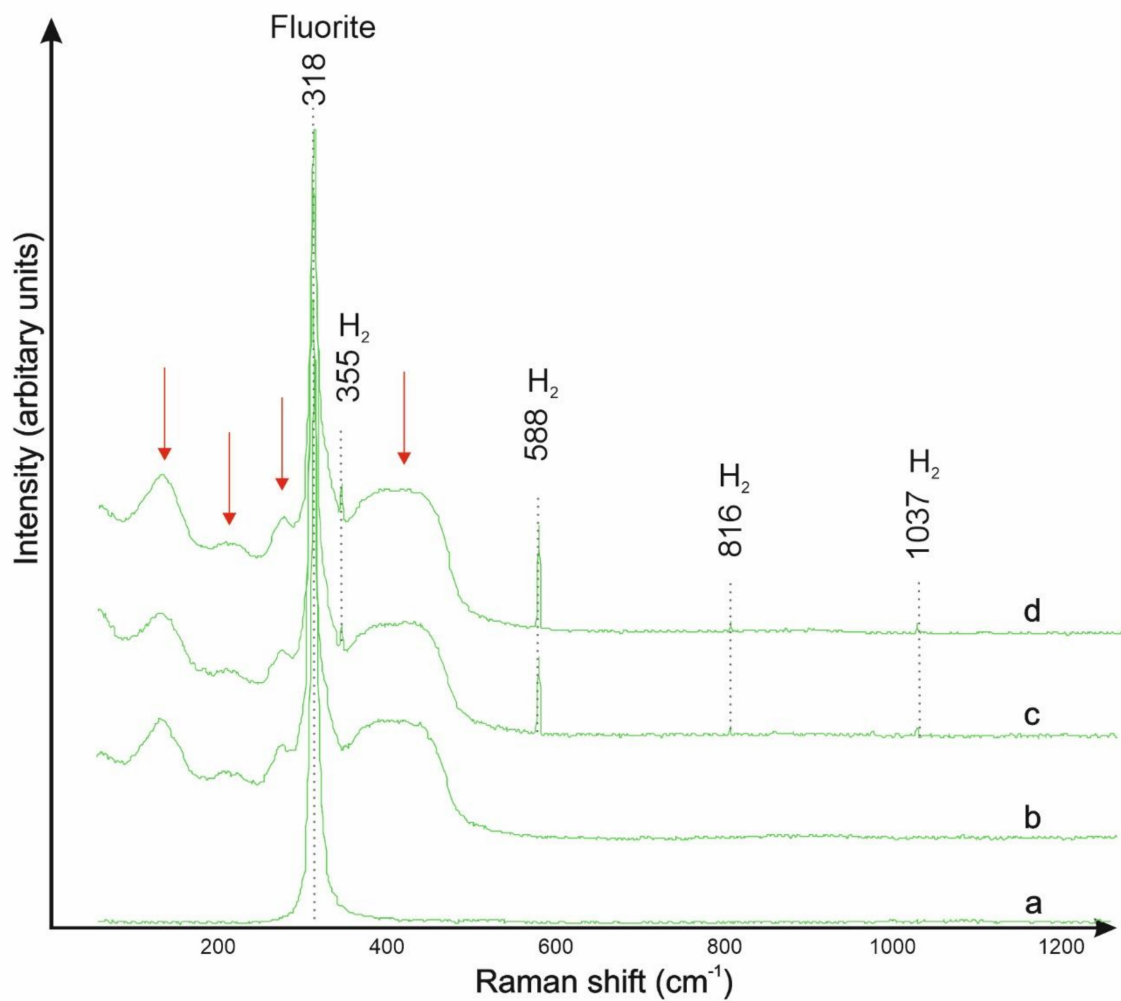


Figure 6. Results of Raman spectroscopy of fluid inclusions and fluorite. (a) Raman spectrum of ordered fluorite; (b) Raman spectrum of the liquid phase in a P inclusion in fluorite; (c) Raman spectrum of the vapor phase of a P inclusion showing the complex rotational band structure of H₂. The Raman band of ordered fluorite is still present, while four other intensities indicate structurally disordered fluorite (indicated by red arrows); (d) Raman spectrum of the vapor phase of an S1 inclusion. The H₂ rotational bands are also observable.

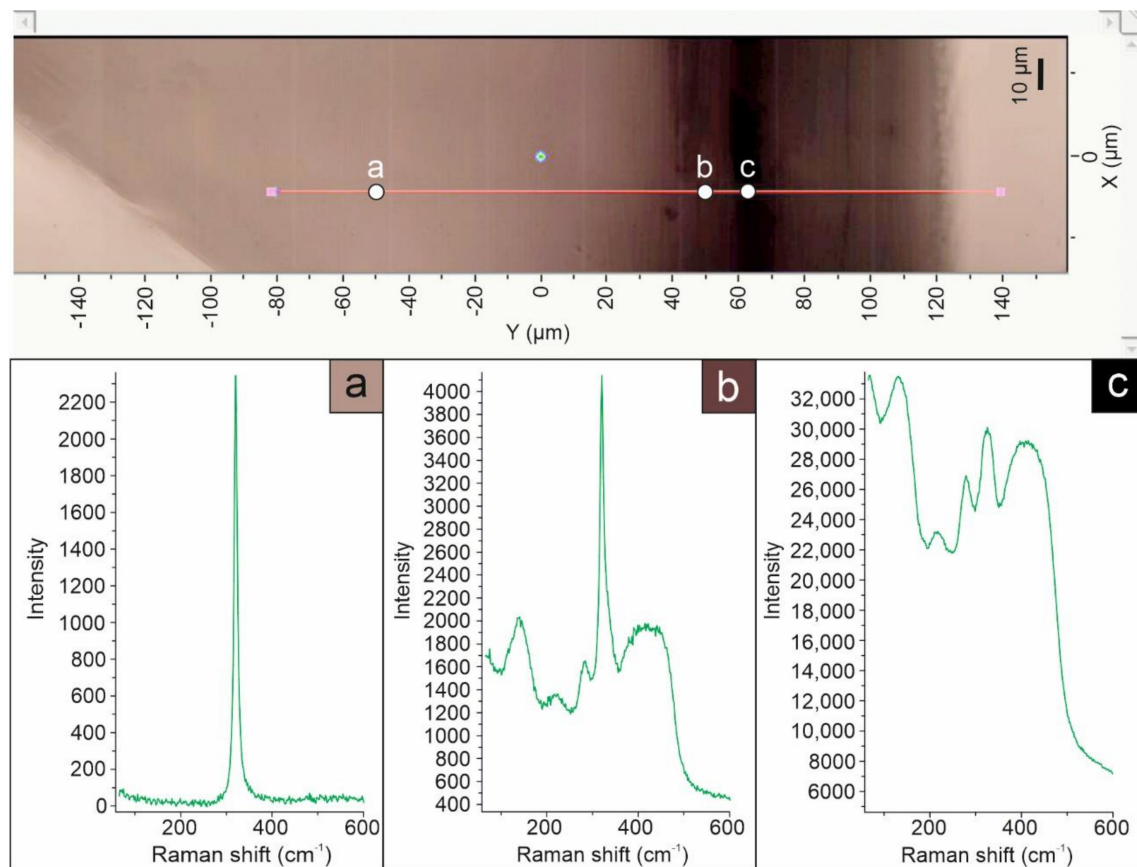


Figure 7. Results of a Raman line scan. (a) In the colorless or pale purple zones, only a sharp fluorite band appears in the spectrum; (b) in the medium purple zone, the fluorite band and the structural damage are also visible; (c) the intensive Raman feature from dark purple zones obscures the fluorite band.

5. Discussion

5.1. Formation Conditions of the Fluorite Veins

Field and petrographic observations support that the fluorite veins cutting the phosphorite layers were formed during low temperature epigenetic hydrothermal processes. The results of fluid inclusion petrography and microthermometry indicate that the primary and the S1 generation of secondary fluid inclusions of fluorite have a similar appearance (size, shape, phase ratio), and their entrapment took place from a homogeneous fluid. Therefore, the homogenization temperatures for the primary fluid inclusions of fluorite can be evaluated as minimum formation temperature of veins, e.g., the minimum temperature of vein formation was most probably between 90 and 130 °C (Figure 5). Much higher temperatures for vein formation are geologically unreasonable, as the isochors of these saline fluid inclusions are fairly steep, and the host rock is non-metamorphosed. The scattering of data toward higher temperatures may reflect some unrecognized “necking down” [33] processes, or temperature fluctuation during the growth of zoned crystals. However, the corroded contour and fragmentation of the fluorite (and dolomite) crystals may suggest that the deformation events resulting in the opening of the veins continued also after the formation of fluorite.

The Σ REE contents are low in the fluorite samples of the study area. Fluorites with low Σ REE are believed to be derived from a sedimentary environment [34]. The low Ce values in the studied fluorites indicate that the high oxygen fugacity in the source of the hydrothermal fluids has led to the Ce^{3+} oxidation and Ce^{4+} immobilization [35]. Additionally, the negative Ce anomaly can be inherited from seawater [36]. This is because marine carbonates show negative Ce anomaly [37]. In addition to low Ce values, the

samples show low REE concentrations. Accordingly, it can be concluded that REE patterns of Pécsely fluorites show that the hydrothermal fluid interacts with marine carbonates, i.e., we may assume that basinal brines are the main source of the mineralization fluids.

The relatively low homogenization temperatures with Ca-enriched, high salinity compositions are similar to fluid inclusion characteristics of saline basinal fluids and especially to Mississippi Valley or Irish Type sediment-hosted epigenetic Pb-Zn ore deposits [38] (Figure 8).

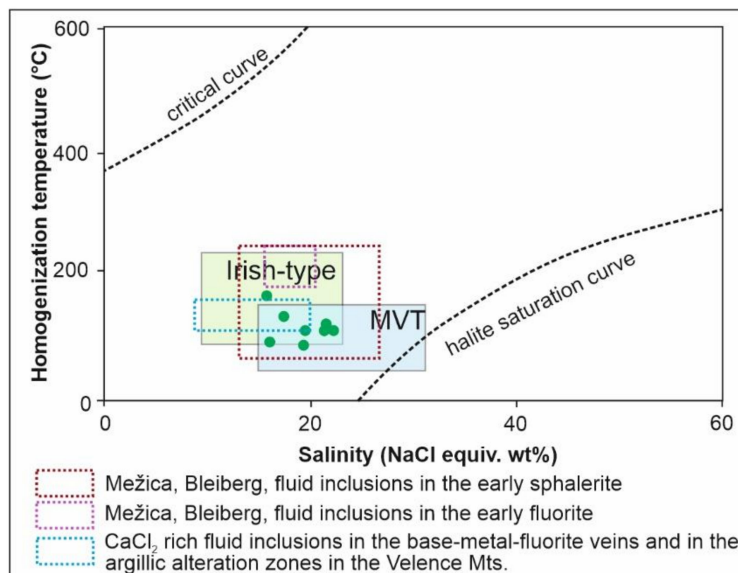


Figure 8. Salinity vs. T_h illustrating typical ranges for inclusions from different types of deposits [38]. For comparison purposes, fluid inclusion data for two Alpine-type epigenetic lead-zinc deposits in the Drau Range (Bleiberg, Mežica) [39], the Pb-Zn-fluorite mineralization of the Velence Mts. [6], and the primary fluid inclusions from Pécsely (green dots) are also shown. Fluid inclusions from Pécsely plot within the MVT field and overlap with data from Mežica, Bleiberg, and Velence Mts.

The microthermometric results of the S1 inclusion generation suggest that the formation of fluorite-containing veins was overprinted by a subsequent, lower temperature fluid flow. The composition of S1 fluid inclusions is almost identical to those of the primary inclusions, while the homogenization temperatures are slightly lower (with 70–80 °C as the most common values) with almost ideal and relatively narrow normal distribution (Figure 5). These properties suggest that S1 inclusions were formed during the waning, lower temperature stage of the same hydrothermal activity, when the infiltrations of a new pulse of the same type of fluid was generated by fracturing of the rocks.

Although the carbon and oxygen isotope data obtained from the carbonates associated with fluorite veins are different from the sedimentary carbonate of the host rock (Figure 9), it is assumed that the fluid ultimately originated from Permian or Triassic buried sea water ($\delta^{18}\text{O}_{\text{SMOW}} \approx 0\text{‰}$, [19]), as no direct magmatic activity has been identified in this period [2,40]. Even during the formation of phosphorite-bearing layers, which preceded the development of the fluorite veins and were contemporary with volcanic activity [2], the magmatic contribution was insignificant to the parent fluid [2]. Nevertheless, the stable isotope compositions of the dolomites associated with fluorite veins overlap with the data from the fracture filling and breccia cementing carbonate of the phosphorite deposit [2] (Figure 9). The negative $\delta^{18}\text{O}$ values might indicate a relatively elevated formation temperature, as utilizing the dolomite–water oxygen fraction equation by [41] and assuming sea water oxygen isotope composition ($\delta^{18}\text{O}_{\text{SMOW}} \approx 0\text{‰}$, [19]) for the parent fluid, the formation temperature is about 70–75 °C. This observation fits well with the assumed evolution of this hydrothermal system because the carbonates represent a later stage in the mineral paragenesis. In

addition, the general morphology of the crystal also suggests slightly elevated temperature, as saddle dolomite is believed to form above 60 °C [27]. Alternatively, it should be assumed an exotic fluid characterized by negative oxygen isotope composition. However, this later scenario is not supported by any evidence.

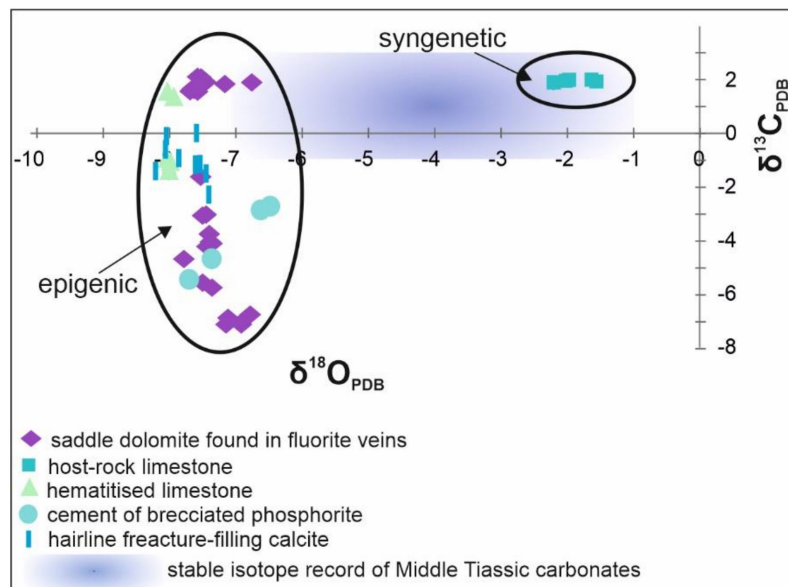


Figure 9. Stable isotope data of calcite grains from fluorite veins are similar to the carbon and oxygen isotopic compositions of the epigenetic calcite crystals found in phosphorite, suggesting their common, hydrothermal origin [2]. In the figure the range of Middle Triassic carbonates is also shown [19].

In contrast to the oxygen isotope composition, the $\delta^{13}\text{C}$ values cover a very wide range from +2.12‰ to −7.16‰. The negative value might be related to organic derived carbon, which can have multiple sources. The first source could be the organic rich phosphorite layers (their TOC—total organic carbon—are 0.58–0.77% [42]), which are cut by the fluorite veins. Another source could be the underlying Permian red sandstone, which is interpreted as a potential source of vein-forming fluid, containing buried plant residuals in addition. The interaction of the fluorite-forming fluid with these formations (Figure 1c) is likely to be responsible for the observed negative $\delta^{13}\text{C}$ values. In addition, the observed variability in carbon isotope composition is probably associated with the degree of this interaction.

5.2. The Origin of H_2 in Fluid Inclusions of Fluorite

Fluorite crystals from the area of Pécsely have a unique characteristic: the presence of H_2 gas in the vapor phase of P and S1 fluid inclusions. The authors of [43,44] examined fluid inclusions in quartz and dolomite grains from Precambrian uranium deposits by Raman spectroscopy, where the inclusions contained H_2 with or without O_2 . Concerning the origin of the gas, it has been concluded that chemical reactions of water or organic matter, nuclear reactions, and indirect chemical reactions of radiolysis processes lead to the enrichment of H_2 and other gases in hydrothermal fluids.

In the Balaton Highland area, the Permian–Triassic sandstone layers in the basement contain traces of redox-front controlled uranium enrichments [18,45], and the phosphorite layers at Pécsely are also enriched in uranium. Therefore, it is plausible to estimate that the hydrothermal fluids responsible for the fluorite mineralization were also interacting with those uranium rich zones and were enriched in hydrogen. However, a model favoring local conditions would be more acceptable regarding the origin of the gas content of the inclusions because fluid inclusions with similar gas content were not described from the Pb–Zn deposits along the PABL (see e.g., [6]). Fluorite and the host rocks at Pécsely have

elevated uranium content; therefore, the presence of hydrogen in fluid inclusions could more probably be related to the in situ (within inclusion) radiolysis of water.

Presumably, the phosphorite strata are responsible for the hydrogen gas in fluid inclusions of fluorite and the structural degradation of the crystals, which were detected during Raman spectroscopic investigation. Due to the direct stratigraphic relationship between fluorite and phosphorite, the radiolysis of fluorite fluid inclusions has been continuous for ~235 million years, which allowed the detection of H₂ despite possible diffusion.

5.3. Metallogenic Implications

The Alpine-Balkan-Carpathian-Dinaride (ABCD) metallogenic and geodynamic provinces include phases of early intracontinental rifting, advanced rifting, oceanization, subduction, and emplacement of ophiolites; collisional and postcollisional deformation events with synkinematic granite plutonism and volcanism; and post-collisional igneous activity [46]. The occurrence of phosphorite layers and fluorite veins are located in the Transdanubian Mountain Range, which is bounded by the Periadriatic Balaton Lineament System (PABL), the most significant shear zone of the ABCD region. The structurally deformed zone of the PABL has been the main channel for magma and fluid flows in various geotectonic environments during and since the Mesozoic era. The formation of Cretaceous lamprophyric magmatism (e.g., Eisenkappel), Paleogene and Neogene intermediate magmatism (e.g., Reck, Velence Mts.), diorite intrusions and stratovolcanoes (e.g., Adamello, Berger plutons, Pohorje intrusions) as well as various types of mineralization (Cu-porphyry, epithermal, epigenetic Pb-Zn) are clearly or apparently controlled by the repeated reactivation of this fault system [6,13,46]. The Triassic rifting and oceanization—associating intensive submarine volcanism—processes took place almost synchronously within the ABCD region, creating carbonate platforms on the passive continental margin. Along the PABL, a number of epigenetic-hydrothermal Pb-Zn ore deposits occur in the Triassic sedimentary rocks of the Northern and Southern Calcareous Alps (e.g., Bleiberg, Mežica, Topla, Raibl, Salafossa) (Figure 10a,b), and apart from the “majors”, there are more than 200 smaller but similar Pb-Zn occurrences known in the region [46]. The ore forming fluids of these deposits are characterized by 122–200 °C and high salinity (7–25 NaCl equivalent wt%) (Figure 8) where the metals were leached and transported by Cl-rich fluids [39,47]. The author of [48] had recognized low-temperature and high salinity calcium-chloride-enriched secondary fluid inclusions in regional-scale distribution in the rock forming quartz of granite in the Velence Mts., which are located about 50 km to the east of the current study area (Figure 1a). Parent fluids of those inclusions were interpreted as “basinal fluids”, and later research by [6] showed that they record a regional fluid flow system of Triassic age, which also produced Pb-Zn mineralization in the Variscan granite of the Velence Mts. Fluorite is also a common mineral in those base-metal rich veins [6] also emphasizing the similarities between those fluids and ore forming fluids of the carbonate hosted lead–zinc mineralizations in the Alps (Figure 8) [39].

The authors of [49,50] investigated the REE geochemistry of fluorite from the Alpine Pb-Zn deposits. Comparing the REE content of fluorite from Pécsely with their results, it can be stated that the fluorite grains contain rare earth elements to a similar extent and distribution as the Alpine specimens (Figure 10c).

The phosphorite occurrence and fluorite veins at Pécsely also show similarities to the Monte San Giorgio (~70 km from Milano to the NNW) occurrence in the Southern Alps. The two areas show similarity not only in the stratigraphic position and formation age of phosphorite horizons but also in the presence of hydrothermal fluorite(-galena-barite) vein mineralization. Galena, barite, and fluorite occur in Monte San Giorgio along faults and dykes, embedded in the volcanic rocks of the Permian and in the overlying Lower and Middle Triassic sediments. The deposits were enriched during the Middle Triassic by hydrothermal fluids moving along tectonic faults [51].

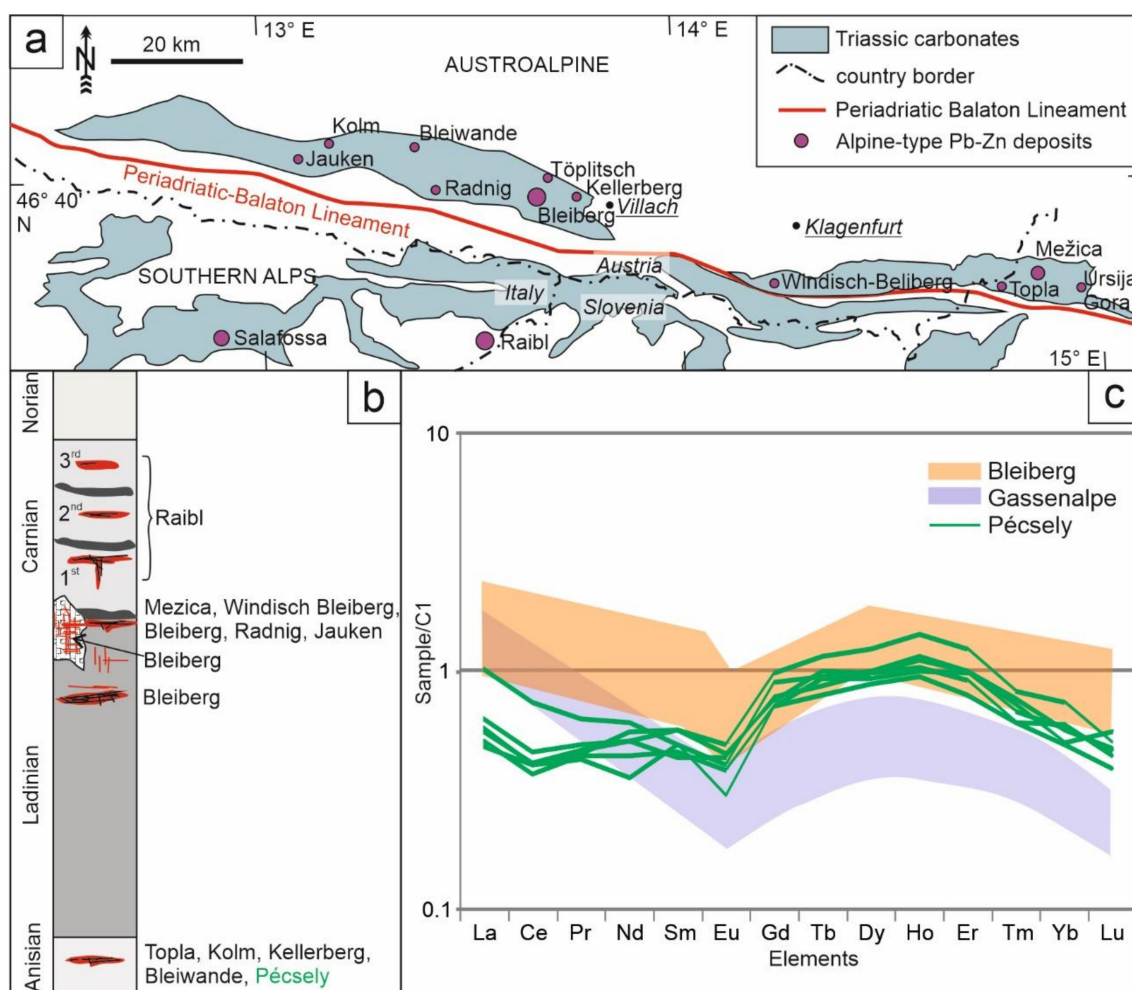


Figure 10. (a) Simplified geological map of the Drau Range after [18,52] showing the positions of the major Alpine-type Pb-Zn deposits; (b) schematic profile showing the positions of the ore-horizons (red lines) in the different stratigraphic niveous (modified after [53]); (c) comparison of the REE content of fluorite from Pécseley with Alpine occurrences [49,50].

The Transdanubian Mountain Range escaped 450–500 km east from the Alpine collision zone during the Late Paleogene–Early Neogene [9]. Accordingly, its original position was located between the South Alpine and Upper East Alpine realm in the Triassic, as a segment of the Adriatic margin of the Neotethys Ocean [54–56]. Our results are consistent with the paleogeographic and geological reconstructions [7,56] too. There are striking similarities between the fluorite veins of Pécseley and certain epigenetic Pb-Zn deposits in the Alps along the PABL, especially regarding fluid inclusion signatures. All this opens up the possibility that a similar type of Alpine-type Pb-Zn deposits may be concealed in the carboniferous sequence of the Transdanubian Mountain Range. However, by far in the absence of a well-established model, this raw material exploration opportunity has not been studied before.

6. Conclusions

Epigenetic-hydrothermal fluorite–carbonate veins and breccias cut across sedimentary phosphorite layers at Pécseley in the Transdanubian Mountain Range Unit of South Alpine affiliation in western Hungary. The results of this study of these veins support the following conclusions:

- The $\delta^{18}\text{O}_{\text{PDB}}$ and $\delta^{13}\text{C}_{\text{PDB}}$ values of carbonate minerals from veins confirm their epigenetic-hydrothermal origin.

- Fluorite from the veins contains REEs in sub-ppm concentration. This low content of REE and their relative concentrations show a good match with the properties of fluorite in the Alpine-type Pb-Zn ore deposits.
- Color zoning of fluorite is associated with defects in the crystal structure.
- The results of fluid inclusion studies indicate that the primary and the S1 generation of secondary fluid inclusions of fluorite have a similar appearance (size, shape, phase ratio), and their entrapment took place from a homogeneous fluid. The relatively low homogenization temperatures with Ca-enriched, high salinity compositions are similar to fluid inclusion characteristics of saline basinal fluids that were also recorded in other areas of the Pannonian Basin and in the Alpine-type Pb-Zn deposits along the Periadriatic-Balaton Lineament
- Fluid inclusions of fluorite contain hydrogen gas; this rather unique feature can be related to the interaction of the parent fluids of the fluorite-bearing veins with the interaction between the fluorite vein-forming epigenetic process and the uranium-bearing phosphorite layers of the host strata and uranium enrichments in the basement rocks and also to the possibly in situ radiolysis of water within the fluid inclusions.

Author Contributions: Conceptualization, Z.M., G.B.K., F.M. and I.D. (István Dódony); methodology, T.V., I.D. (István Dunkl), F.Z., G.C. and G.B.K.; formal analysis, Z.M., T.V., I.D. (István Dunkl), F.Z. and G.C.; investigation, Z.M., T.V., I.D. (István Dunkl), F.Z., G.C. and G.B.K.; writing—original draft preparation, Z.M. and G.B.K.; writing—review and editing, F.M., T.V., I.D. (István Dunkl), F.Z., G.C. and I.D. (István Dódony); visualization, Z.M., I.D. (István Dunkl), F.M., G.B.K., T.V., F.Z., and G.C.; supervision, G.B.K., I.D. (István Dódony) and F.M.; funding acquisition, G.B.K., Z.M. and F.M. All authors have read and agreed to the published version of the manuscript.

Funding: This study was partly supported by TÁMOP-3.3.21-15/1 research grant no. NTP-NFTÖ-16-1032. Finalization and publication of this research is supported by the ENeRAG project, which has received funding from the European Union’s Horizon 2020 research and innovation program under grant agreement No 810980.

Data Availability Statement: The data presented in this study are available within this article.

Acknowledgments: We wish to say thanks to all colleagues who contributed to this work: Zsolt Bendő, Ágnes Takács, and Sándor Klaj. The authors are grateful to three anonymous reviewers for the careful and critical review of the manuscript and for their useful suggestions. The University Centrum of Applied Geosciences (UCAG) is thanked for the access to the E. F. Stumpfl Electron Microprobe Laboratory, Leoben. The ELTE Faculty of Science Research Instrument Core Facility is thanked for the access to the Raman laboratory. The LA-ICP-MS measurements were performed at the University of Göttingen. The Institute for Geological and Geochemical Research Centre for Astronomy and Earth Sciences, which is part of the Eötvös Loránd Research Network, is thanked for the stable isotope analyses. The SEM-CL imaging was available thanks to the KMOP-4.2.1/B-10-2011-0002 grant by the European Union, co-financed by the European Social Fund.

Conflicts of Interest: The authors declare no conflict of interest. The funders had no role in the design of the study; in the collection, analyses, or interpretation of data; in the writing of the manuscript, or in the decision to publish the results.

References

1. Kiss, J.; Virágh, K. A uranium-bearing phosphatic rock in the Triassic of the Balaton Uplands around Pécsely. *Bull. Hung. Geol. Soc.* **1959**, *89*, 85–97.
2. Molnár, Z.; Kiss, B.G.; Dunkl, I.; Czuppon, G.; Zaccarini, F.; Dódony, I. Geochemical characteristics of Triassic and Cretaceous phosphorite horizons from the Transdanubian Mountain Range (western Hungary): Genetic implications. *Mineral. Mag.* **2018**, *82(S1)*, S147–S171. [[CrossRef](#)]
3. Frisch, W.; Kuhlemann, J.; Dunkl, I.; Brügel, A. Palinspastic reconstruction and topographic evolution of the Eastern Alps during late Tertiary extrusion. *Tectonophysics* **1998**, *297*, 1–15. [[CrossRef](#)]
4. Fodor, L.; Csontos, L.; Bada, G.; Györfi, I.; Benkovics, L. Tertiary tectonic evolution of the Pannonian basin system and neighbouring orogens: A new synthesis of paleostress data. In *The Mediterranean Basins: Tertiary Extension within the Alpine; Orogen, B., Durand, L., Jolivet, F., Horváth, M., Séranne, Eds.; Geological Society Special Publications: London, UK, 1999; Volume 156, pp. 295–334.*

5. Haas, J.; Mioč, P.; Tomljenović, B.; Árkai, P.; Bércziné Makk, A.; Koroknai, B.; Kovács, S.; Rálich-Felgenhauer, E. Complex structural pattern of the Alpine Dinaridic–Pannonian triple junction. *Int. J. Earth Sci.* **2000**, *89*, 377–389. [[CrossRef](#)]
6. Benkó, Z.; Molnár, F.; Lespinasse, M.; Billström, K.; Pécskay, Z.; Németh, T. Triassic fluid mobilization and epigenetic lead-zinc sulphide mineralization in the Transdanubian Shear Zone (Pannonian Basin, Hungary). *Geol. Carpath.* **2014**, *65*, 177–194. [[CrossRef](#)]
7. Kázmér, M.; Kovács, S. Permian-Paleogene paleogeography along the eastern part of the Insubric-Periadriatic lineament system: Evidence for continental escape of the Bakony-Drauzug unit. *Acta Geol. Hung.* **1985**, *28*, 71–84.
8. Csontos, L.; Nagymarosy, A.; Horváth, F.; Kovács, M. Tertiary evolution of the Intracarpathian area: A model. *Tectonophysics* **1992**, *208*, 221–241. [[CrossRef](#)]
9. Tari, G.; Bada, G.; Beidinger, A.; Csizmeg, J.; Danišik, M.; Gjerazi, I.; Grasemann, B.; Kováč, M.; Plašienka, D.; Šujan, M.; et al. The connection between the Alps and the Carpathians beneath the Pannonian Basin: Selective reactivation of Alpine nappe contacts during Miocene extension. *Glob. Planet. Chang.* **2021**, *197*, 103401. [[CrossRef](#)]
10. Tari, G. Nealpine tectonics of the Danube Basin (NW Pannonian Basin, Hungary). In *Peri-Tethys Memoir 2: Structure and Prospects of Alpine Basins and Forelands*; Ziegler, P.A., Horváth, F., Eds.; Mémoires du Muséum National d’histoire Naturelle: Washington, DC, USA, 1996; Volume 170, pp. 439–454.
11. Csontos, L.; Vörös, A. Mesozoic plate tectonic reconstruction of the Carpathian region. *Palaeogeogr. Palaeoclimatol. Palaeoecol.* **2004**, *210*, 1–56. [[CrossRef](#)]
12. Kovács, I.; Szabó, C.; Bali, E.; Falus, G.; Benedek, K.; Zajacz, Z. Palaeogene—Early Miocene igneous rocks and geodynamics of the Alpine—Carpathian Dinaric region: An integrated approach. *Geol. Soc. Am. Spec. Pap.* **2007**, *418*, 93–112.
13. Köppel, V. Summary of lead isotope data from ore deposits of the Eastern and Southern Alps: Some metallogenic and geotectonic implications. In *Mineral Deposits of the Alpine Epoch in Europe*; Schneider, H.J., Ed.; Springer: Berlin/Heidelberg, Germany, 1983; pp. 162–269.
14. Budai, T.; Haas, J. Triassic sequence stratigraphy of the Balaton Highland, Hungary. *Acta Geol. Hung.* **1997**, *40*, 307–335.
15. Budai, T.; Vörös, A. Middle Triassic history of the Balaton Highland: Extensional tectonics and basin evolution. *Acta Geol. Hung.* **1992**, *35*, 237–250.
16. Budai, T.; Vörös, A. Middle Triassic platform and basin evolution of the Southern Bakony Mountains (Transdanubian Range, Hungary). *Riv. Ital. Paleont. Stratigr.* **2006**, *112*, 359–371.
17. Budai, T.; Császár, G.; Csillag, G.; Dudko, A.; Koloszár, L.; Majoros, G. *Geology of the Balaton Highland. Explanation to the Geological Map of the Balaton Highland, 1:50,000*; Occasional Papers; Hungarian Geological Institute: Budapest, Hungary, 1999; Volume 197, p. 257.
18. Schroll, E.; Rantitsch, G. Sulphur isotope patterns from the Bleiberg deposit (Eastern Alps) and their implications for genetically affiliated lead-zinc deposits. *Mineral. Petrol.* **2005**, *84*, 18. [[CrossRef](#)]
19. Korte, C.; Kozur, H.W.; Veizer, J. $\delta^{13}\text{C}$ and $\delta^{18}\text{O}$ values of Triassic brachiopods and carbonate rocks as proxies for coeval seawater and palaeotemperature. *Palaeogeogr. Palaeoclimatol. Palaeoecol.* **2005**, *226*, 287–306. [[CrossRef](#)]
20. Hall, D.L.; Sterner, S.M.; Bodnar, R.J. Freezing point depression of NaCl-KCl-H₂O solutions. *Econ. Geol.* **1988**, *83*, 197–202. [[CrossRef](#)]
21. Naden, J. CalcicBrine: A Microsoft Excel 5.0 add-in for calculating salinities from microthermometric data in the system NaCl–CaCl₂–H₂O. In Proceedings of the Program and Abstracts of Biennial Pan-American Conference on Research on Fluid Inclusions, Madison, WI, USA, 30 May–1 June 1996.
22. Potter, R.W., II; Clyne, M.A. Pressure correction for fluid inclusion homogenization temperature. In Proceedings of the Programs and Abstracts, International Association Genesis Ore Deposits Symposium, Snowbird, Alta, UT, USA, 14–19 August 1978; p. 146.
23. Zhang, Y.G.; Frantz, J.D. Determination of homogenization temperatures and densities of supercritical fluids in the system NaCl-KCl-CaCl₂-H₂O using synthetic fluid inclusions. *Chem. Geol.* **1987**, *64*, 335–350. [[CrossRef](#)]
24. Wolff, R.; Dunkl, I.; Kempe, U.; von Eynatten, H. The age of the latest thermal overprint of tin and polymetallic deposits in the Erzgebirge, Germany: Constraints from Fluorite (U-Th-Sm)/He Thermochronology. *Econ. Geol.* **2015**, *110*, 2025–2040. [[CrossRef](#)]
25. McDonough, W.F.; Sun, S.S. The composition of the Earth. *Chem. Geol.* **1995**, *120*, 223–253. [[CrossRef](#)]
26. McLennan, S.M. Relationships between the trace element composition of sedimentary rocks and upper continental crust. *Geochem. Geophys.* **2001**, *2*, 1–24. [[CrossRef](#)]
27. Spötl, C.; Wennemann, T.W. Continuous-flow isotope ratio mass spectrometric analysis of carbonate minerals. *Rapid. Commun. Mass. Spectrom.* **2003**, *17*, 1004–1006. [[CrossRef](#)] [[PubMed](#)]
28. Vanko, D.A.; Bodnar, R.J.; Sterner, S.M. Synthetic fluid inclusions: VIII. Vapor-saturated halite solubility in part of the system NaCl-CaCl₂-H₂O, with application to fluid inclusions from oceanic hydrothermal systems. *Geochim. Cosmochim. Acta* **1988**, *52*, 2451–2456. [[CrossRef](#)]
29. Oakes, C.S.; Bodnar, J.R.; Simonson, J.M. The system NaCl-CaCl₂-H₂O: I. The ice liquidus at 1 atm total pressure. *Geochim. Cosmochim. Acta* **1990**, *54*, 603–610. [[CrossRef](#)]
30. Mernagh, T.P.; Wilde, A.R. The use of the Raman microprobe for the determination of salinity in fluid inclusions. *Geochim. Cosmochim. Acta* **1989**, *53*, 765–771. [[CrossRef](#)]
31. Sun, Q.; Zhao, L.; Li, N.; Liu, J. Raman spectroscopic study for the determination of Cl[−] concentration (molarity scale) in aqueous solutions: Application to fluid inclusions. *Chem. Geol.* **2010**, *272*, 55–61. [[CrossRef](#)]

32. Čermáková, Z.; Bezdička, P.; Němec, I.; Hradilová, J.; Šrein, V.; Blažek, J.; Hradil, D. Naturally irradiated fluorite as a historic violet pigment: Raman spectroscopic and X-ray diffraction study. *J. Raman Spectrosc.* **2015**, *46*, 236–243. [[CrossRef](#)]
33. Roedder, E. Fluid Inclusions. *Rev. Mineral.* **1984**, *12*, 644.
34. Hill, G.T.; Andrew, R.C.; Philip, R.K. Geochemistry of southwestern New Mexico fluorite occurrences: Implications for precious metals exploration in fluorite-bearing systems. *J. Geochem. Explor.* **2000**, *68*, 1–20. [[CrossRef](#)]
35. Constantopoulos, J. Fluid inclusions and rare earth element geochemistry of fluorite from south-central Idaho. *Econ. Geol.* **1988**, *83*, 626–636. [[CrossRef](#)]
36. Castorina, F.; Masi, U.; Padalino, G.; Palomba, M. Trace-element and Sr–Nd isotopic evidence for the origin of the Sardinian fluorite mineralization (Italy). *Appl. Geochem.* **2008**, *23*, 2906–2921. [[CrossRef](#)]
37. Parekh, P.P.; Möller, P.; Dulski, P. Distribution of trace elements between carbonate and non-carbonate phases of limestone. *Earth. Planet. Sci. Lett.* **1977**, *34*, 39–50. [[CrossRef](#)]
38. Wilkinson, J.J. Fluid inclusions in hydrothermal ore deposits. *Lithos* **2001**, *55*, 229–272. [[CrossRef](#)]
39. Kuhlemann, J.; Vennemann, T.; Herlec, U.; Zeeh, S.; Bechstädt, T. Variations of sulfur isotopes, trace element compositions, and cathodoluminescence of Mississippi Valley type lead-zinc ores from the Drau-Range, Eastern Alps (Slovenia—Austria): Implications for ore deposition on a regional versus micro scale. *Econ. Geol.* **2001**, *96*, 1931–1941.
40. Dunkl, I.; Farics, É.; Józsa, S.; Lukács, R.; Haas, J.; Budai, T. Traces of Carnian volcanic activity in the Transdanubian Range, Hungary. *Int. J. Earth Sci.* **2019**, *108*, 1451–1466. [[CrossRef](#)]
41. Horita, J. Oxygen and carbon isotope fractionation in the system dolomite-water-CO₂ to elevated temperatures. *Geochim. Cosmochim. Acta* **2014**, *129*, 111–124. [[CrossRef](#)]
42. Budai, T.; Haas, J.; Vörös, A.; Molnár, Z. Influence of upwelling on the sedimentation and biota of the segmented margin of the western Neotethys: A case study from the Middle Triassic of the Balaton Highland. *Facies* **2017**, *63*, 22. [[CrossRef](#)]
43. Dubessy, J.; Pagel, M.; Beny, J.M.; Christensen, H.; Hickel, B.; Kosztolanyi, C.; Poty, B. Radiolysis evidenced by H₂-O₂ and H₂-bearing fluid inclusions in three uranium deposits. *Geochim. Cosmochim. Acta* **1988**, *52*, 1155–1167. [[CrossRef](#)]
44. Richard, A. Radiolytic (H₂, O₂) and other trace gases (CO₂, CH₄, C₂H₆, N₂) in fluid inclusions from unconformity related U deposits. *Procedia Earth Planet. Sci.* **2017**, *17*, 273–276. [[CrossRef](#)]
45. Majoros, G. Problems of Permian sedimentation in the Transdanubian Central Mountains: A palaeogeographic model and some conclusions. *Bull. Hung. Geol. Soc.* **1980**, *110*, 323–341.
46. Palinkaš, L.A.; Damyranov, Z.K.; Borojević Šoštarić, S.; Strmić Palinkaš, S.; Marinova, I. Divergent drift of Adriatic-Dinaridic and Moesian carbonate platforms during the rifting phase witnessed by triassic MVT Pb-Zn and SEDEX deposits; a metallogenic approach. *Geol. Croat.* **2016**, *69*, 75–78. [[CrossRef](#)]
47. Schroll, E. Alpine type Pb-Zn-deposits (APT) hosted by Triassic carbonates. In *Mineral Deposit Research: Meeting the Global Challenge, Proceedings of the Eighth Biennial SGA Meeting, Beijing, China, 18–21 August 2005*; Springer: Berlin/Heidelberg, Germany, 2005; pp. 175–178.
48. Molnár, F. Characteristics of Variscan and Palaeogene fluid mobilization processes in the Velence Mts., Hungary: A comparative fluid inclusion study. *Acta Mineral. Petrogr.* **2004**, *45*, 55–63.
49. Hein, U.F.; Schneider, H.J. Fluorine Anomalies Accompanying the Alpine Pb-Zn Deposits Compared to the Geochemistry of Their Fluorites. In *Mineral Deposits of the Alps and of the Alpine Epoch in Europe*; Special Publication No. 3 of the Society for Geology Applied to Mineral Deposits; Schneider, H.J., Ed.; Springer: Berlin/Heidelberg, Germany, 1983.
50. Möller, P.; Morteani, G. On the geochemical fractionation of rare earth elements during the formation of Ca minerals and its application to problems of the genesis of ore deposits. In *The Significance of Trace Elements in Solving Petrogenetic Problems and Controversies*; Augustithis, S.S., Ed.; Theophrastus Publications: Athens, Greece, 1983; pp. 747–791.
51. Oppizzi, P.; Camana, G.; Neri, P.; Rossi, C.; Rodeghiero, F.; Bernasconi, E. Le mineralizzazioni a barite e fluorite del Monte San Giorgio (Canton Ticino meridionale). *Geol. Insubrica* **1999**, *4*, 79–89.
52. Bigi, G.; Castellarin, A.; Coli, M.; Dal Piaz, G.V.; Vai, G.B. Structural Model of Italy scale 1:500,000, sheet 2. C.N.R. *Progett. Final. Geodin.* **1990**, *114*. [[CrossRef](#)]
53. Cerny, I. Die karbonatgebundenen Blei-Zink-Lagerstätten des alpinen und ausser-alpinen Mesozoikums; Die Bedeutung ihrer Geologie, Stratigraphie und Faziesgebundenheit fuer Prospektion und Bewertung. Carbonate-bound lead-zinc deposits of the Alpine and extra-Alpine Mesozoic; implications for prospecting and evaluation of their stratigraphy and facies relationships. *Arch. für Lagerstättenforschung Geol. Bundesanst.* **1989**, *11*, 5–125.
54. Haas, J.; Kovács, S.; Krystyn, L.; Lein, R. Significance of Late Permian–Triassic facies zones in terrane reconstructions in the Alpine—North Pannonian domain. *Tectonophysics* **1995**, *242*, 19–40. [[CrossRef](#)]
55. Mandl, G.W. The Alpine sector of the Tethyan shelf—examples of Triassic to Jurassic sedimentation and deformation from the Northern Calcareous Alps. *Mitt. Gesellsch. Geol. Bergb. Öst.* **2000**, *92*, 61–77.
56. Gawlick, H.J. Paläogeographie der Ober-Trias Karbonatplattform in den Nördlichen Kalkalpen. *Mitt. Gesellsch. Geol. Bergb. Öst.* **2000**, *44*, 45–95.